RSC Advances

PAPER

View Article Online
View Journal | View Issue

Cite this: *RSC Adv.*, 2014, **4**, 47234

Highly crystalline urchin-like structures made of ultra-thin zinc oxide nanowires†

Anisha Gokarna,*[a] Romain Parize,[a] Hind Kadiri,[a] Komla Nomenyo,[a] Gilles Patriarche,[b] Patrice Miska[c] and Gilles Lerondel*[a]

Received 27th June 2014
Accepted 18th September 2014

DOI: 10.1039/c4ra06327a

www.rsc.org/advances

We report the synthesis of ultra-thin, monocrystalline, highly luminescent ZnO nanowires (NWs) on polystyrene (PS) beads as templates. The synthesis of these NWs on PS beads was conducted by the chemical bath deposition technique in the absence of any catalysts or additives. They have an average diameter of 15 nm (depending on the concentration of the solution) and an average length of 500 nm. Structural characterization reveals that these NWs are monocrystalline, with a hexagonal phase and grow along the [0001] direction. Photoluminescence measurements of these unannealed, ultra-thin NWs exhibit a strong ultra-violet emission at room temperature with an internal quantum efficiency of 23%. We show that the concentration of the aqueous solution plays a key role in controlling the size of the NWs.

Introduction

Zinc oxide is one of the most promising functional materials because of its catalytic, electrical, optoelectronic, and piezoelectric properties.[1] Especially, one-dimensional (1D) ZnO nanostructures have attracted much attention owing to their applications in nanodevices such as light-emitting diodes,[2,3] field-effect transistors,[4–6] ultraviolet lasers,[7,8] chemical sensors,[9,10] and solar cells.[11–13] However, there are two prerequisites for the realization of ZnO nanodevices. One is the development of a simple and low-cost method of synthesizing ZnO nanomaterials for industrial mass production. Various synthesis methods have been developed for 1D ZnO nanomaterial growth, including physical vapor deposition,[14–16] chemical vapor deposition,[17–19] laser ablation,[20] and the solution method.[21–23] The solution method has the merits of low temperature, large scale, and low-cost synthesis. The other prerequisite for ZnO nanodevice application is the ability to control the position and morphology of the ZnO nanostructures. Various techniques have been used for the selective patterned growth of ZnO nanostructures. The most commonly used was the Vapor–Liquid–Solid (VLS) technique. However, the VLS growth method requires relatively high synthesis temperature, and also, catalyst particles remain at the tip of the grown nanocrystals. More recently, researchers have been using a solution growth method in combination with photolithography or e-beam lithography for patterning.[24]

Patterned arrays of 1D ZnO NWs have a promising future as applications in electronic and optoelectronic devices, because they are expected to improve the performance of various nanodevices. Recently, many efforts have focused on the integration of 1D nanoscale building blocks into 3D architectures. Urchin-like ZnO NWs that combine properties of 3D and 1D materials may emerge as a more interesting alternative than simple arrays of NWs due to the higher specific surface and porosity,[25] especially for application in dye and semiconductor-sensitized solar cells.[26,27] J. Elias *et al.* reported the formation of hollow urchin-like ZnO NWs by electrochemical deposition.[28–30] The average diameter of the NWs achieved was ~220 nm. Diameter-controlled synthesis of well-aligned small-diameter ZnO nanowire arrays by catalyst-free methods is still a major challenge. Ultra-thin NWs are extremely important due to the fact that as the diameter of the NWs decreases, quantum confinement and surface effects start gaining prominence.[31] These effects modify the electronic and chemical properties of the nanomaterials. Another important quantum mechanical feature in NWs is the phonon confinement effect as many material properties, such as thermal transport, can be understood in terms of phonons.[32]

In this article we successfully synthesized, well-aligned, small diameter ZnO NWs with controlled core dimensions, on PS beads. A simple low-cost, catalyst-free chemical bath deposition technique was used for their patterned growth on PS beads. E-beam lithography or optical lithography techniques were not utilized for the patterning process. These as-grown,

[a]*Laboratoire de Nanotechnologie et d'Instrumentation Optique, Institut Charles Delaunay, CNRS UMR 6281, Université de Technologie de Troyes, 12 rue Marie Curie, BP 2060, 10010 Troyes, France. E-mail: anisha.gokarna@utt.fr; lerondel@utt.fr*

[b]*Laboratory of Photonics and Nanostructures, UPR-20, Site Alcatel de Marcoussis, Route de Nozay, 91460 Marcoussis, France*

[c]*Institut Jean Lamour – CNRS UMR 7198 – Université de Lorraine, Faculté des Sciences et Technologies, BP 70239, F-54506 Vandoeuvre les Nancy, France*

† Electronic supplementary information (ESI) available. See DOI: 10.1039/c4ra06327a

unannealed, urchin-like, ultra-thin ZnO NWs were studied in details in terms of their structural and optical properties.

Experimental section

A Self-assembled patterning of PS beads by dip coating

Carboxylate-modified polystyrene beads having a diameter of 2 μm were purchased from Fisher Scientific. The substrates used were undoped p-type (100) silicon wafers which were cleaned with ethanol and de-ionized water. 400 μL of the beads solution was mixed with the same volume of ethanol by using a micropipet. This mixed solution was deposited drop by drop onto the surface of de-ionized water in a small Petri dish. The carboxylate-modified PS beads self assembled onto the surface of water as they were hydrophobic. A Silicon substrate was slowly dipped into the solution at an angle of 45°, and then slowly removed from the solution. A self organization of PS beads on silicon was observed after this dip coating process. The sample is then allowed to dry in air for a short period of time. The PS beads deposited on silicon are then heated in an oven at 100 °C.

B Synthesis of ZnO seed layer

The seed layer is prepared by mixing a solution containing zinc acetate and ethanol to form a 0.48 M solution. This solution is stirred for a time period of 24 h. The seed layer is then deposited on the PS beads by spin coating technique. Thereafter, the PS beads with the freshly deposited seed layer are annealed on a hot plate at 225 °C.

C Synthesis of ZnO urchin-like structures on PS beads

The growth of ZnO NWs on the PS beads is conducted by chemical bath deposition technique. 0.018 M zinc acetate was dissolved in 250 ml of water. 1 ml of ammonium hydroxide was added to this solution and stirred at room temperature. Synthesis is conducted in the absence of metal catalysts or additives. This mixed solution is heated at 87 °C in a three neck round bottom flask. The sample consisting of the PS beads and the ZnO seed layer deposited above it is immersed in this solution for a time period of 35 min. Thereafter, the sample is washed with water and dried in air. Two other molar concentrations of 0.029 M and 0.02 M, respectively were also used for the synthesis of the ZnO NWs.

D Structural and optical characterization

All the samples are observed with an SEM to check the growth and the size of the ZnO nanorods.

The surface morphology and the cross section of the ZnO NWs on PS beads was examined using a scanning electron microscope (SEM, HITACHI S-3400N, 30 kV). The crystallinity of the nanostructures were measured by XRD. High resolution TEM (JEOL 2200FS) which was equipped with a high angle annular dark field detector (HAADF) and energy dispersive X-ray spectroscopy was also used for studying the structural characteristics of the NWs. The optical properties of the samples were studied at room temperature by photoluminescence (PL) spectroscopy using a He–Cd laser (325 nm) as an excitation source, and a CCD camera as a detector. An unfocused laser beam was used for the PL studies. A 32 cm focal length spectrometer with a 150 lines/mm grating was used for PL spectroscopy.

Results and discussion

A Structural properties

The morphology and the average size of the patterned NWs were studied by SEM. Fig. 1 shows a low magnification SEM image of uniform, vertically-aligned, urchin-like ZnO NWs completely covering a spherical PS bead which was coated with a ZnO seed layer. The PS bead size in this case was around 1.8 μm. The NWs are radially pointing outwards.

At high magnification (Fig. 2), it is observed that the ultra-thin NWs have a minimum diameter of about 9 nm and a size distribution in the range of 9–30 nm. Inset in Fig. 2 shows a diameter histogram of the ZnO NWs size distribution wherein we observe NWs average size is around 15 nm (inset of Fig. 2). The average length of the NWs is 500 nm, however the NWs with small diameter are less than 200 nm in length. The density of the NWs is quite high. As per our calculation, on a single PS bead with a diameter of 2 microns, covered by ZnO NWs having an approx. Length of 500 nm and diameter of 10 nm, the number of NWs grown are 1.6×10^5.

To confirm the phase composition and the crystallinity of the synthesized nanostructres, we have conducted XRD pattern analysis. Fig. 3 shows the XRD pattern of the NWs grown at a concentration of 0.018 M.

All of the diffraction peaks of the XRD patterns are indexed to a wurtzite hexagonal structure. The diffraction pattern indicates pure and good crystallinity of the ZnO nanostructures with the

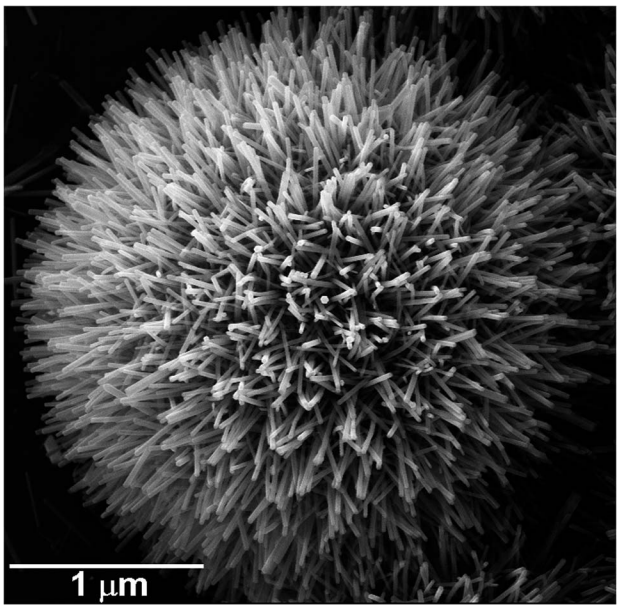

Fig. 1 SEM image of urchin-like ultra-thin ZnO NWs synthesized on PS beads as templates.

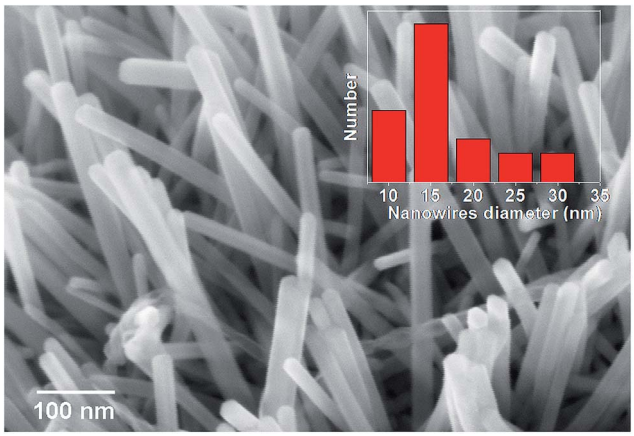

Fig. 2 High-magnification SEM image of the NWs growing on PS bead coated with ZnO seed layer. The inset shows the diameter distribution of the ZnO NWs grown at a low zinc ion concentration.

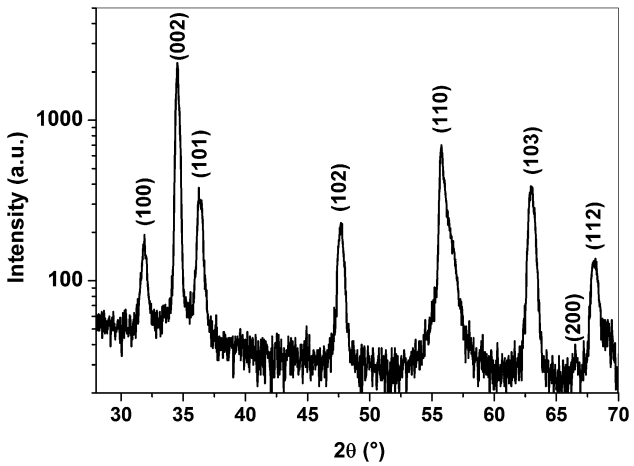

Fig. 3 A representative XRD pattern of ultra-thin crystalline ZnO NWs grown at a low concentration of 0.018 M.

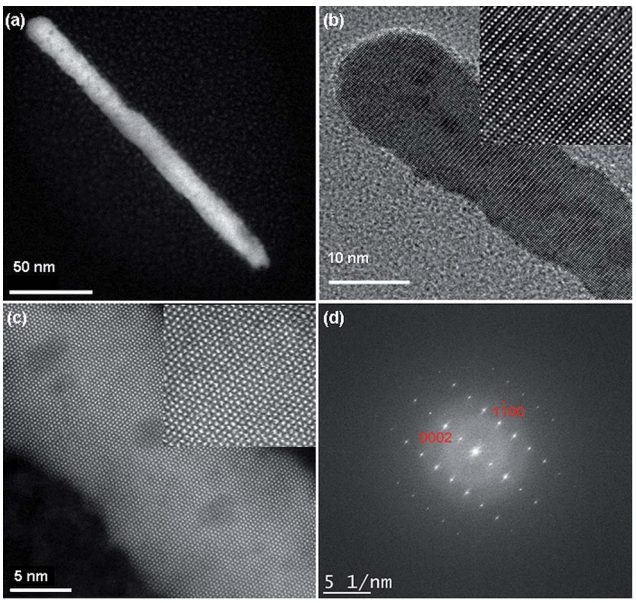

Fig. 4 (a) STEM images of ZnO ultra-thin NW with a diameter of less than 15 nm. (b) HRTEM image of the nanowire and (c) HAADF-STEM image showing the atoms in the NW. Insets in (b) and (c) show the lattice planes and the atoms, respectively.(d) FFT pattern obtained from the HRTEM image 4b indicates that the growth axis of the nanowire is ⟨0001⟩.

absence of other compounds. The NWs are highly crystalline even though the sample is not annealed. The intensity of the (0002) peak in the XRD pattern is very strong compared to those of other peaks which is an evidence that the nanorods have a preferred orientation along *c*-axis. (0002) Structural analysis using TEM was also carried out on the ZnO NWs as seen in Fig. 4. Fig. 4a is a HAADF-STEM image of a single nanowire of diameter approx. 10 nm. The nanowire is oriented along the ⟨11–20⟩ zone axis. The axis of growth is ⟨0001⟩. The edge as well as the facets of the nanowire show some roughness. Fig. 4b represents a high resolution transmission electron microscopy (HRTEM) image of the nanowire. One can observe the (0002) ZnO lattice fringes with an interplanar spacing of 0.26 nm as clearly observed in the inset in Fig. 4b. This indicates that the ZnO NW is a high-quality, monocrystalline wire with a preferential growth along the [0001] direction. It is also observed that the NW ends with a rounded head encapsulated by high-index crystal planes (Fig. 4b). Fig. 4c shows an HAADF-STEM image of the same nanowire. The HAADF contrast depends on the zinc atoms. On the HAADF images with an atomic resolution, we observe crystal structure until the edge of the NW. The darker spots observed in Fig. 4a–c arise from the surface roughness. This surface roughness can be observed on the edges too. Inset in Fig. 4c is a magnified image of the HAADF-STEM image showing the atoms. Fig. 4d shows the Fast Fourier Transform image obtained from the HRTEM images. This FFT pattern indicates that the hexagonal ZnO nanorod grows along the [001] direction.

B Optical properties

PL spectroscopy technique was used in order to further analyse these NWs. Typical PL spectra obtained at four different temperatures are shown in Fig. 5a. The inset shows the intensity of the PL emission in logarithmic scale as a function of the energy.

The dominant band in our sample is a characteristic near band-edge (NBE) emission which is observed in the range 3.28 eV (377 nm) to 3.36 eV (368 nm) depending on the temperature (*T*). Apart from the NBE emission, a weak emission band centred around 2.31 eV (535 nm) is also observed. This band is a deep level (DL) emission band and is assigned to the oxygen vacancies.[33–36]

In order to further study the NBE emission we investigated the peak position as a function of the temperature *T* and the peak intensity as a function of 1/*T*. Fig. 5b and c show the NBE peak position and intensity as a function of *T* and 1/*T*, respectively. The peak position as a function of *T* was fitted using the Varshni empirical equation defined as follow:

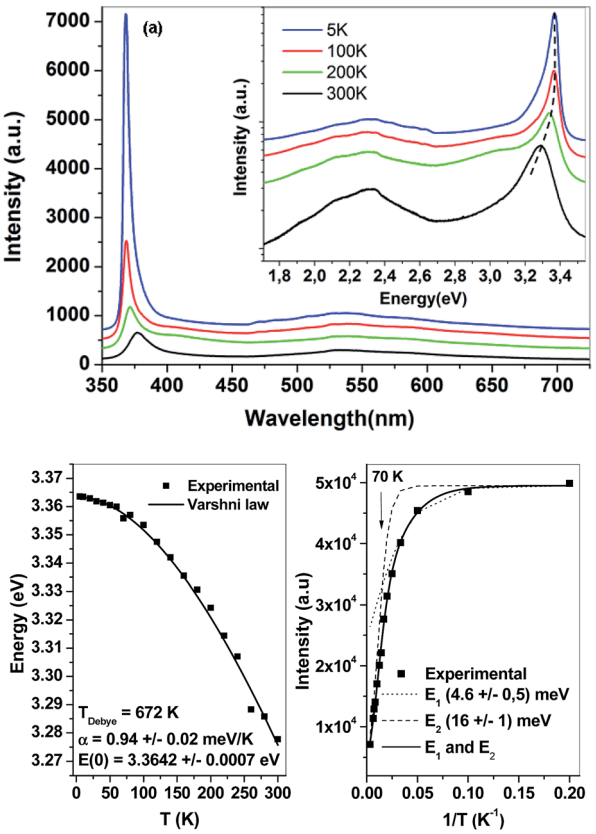

Fig. 5 Photoluminescence properties of the ultra narrow ZnO NWs grown on PS beads (lowest concentration). (a) Typical PL spectra for 4 different temperatures as indicated. Inset shows the same spectra but in logarithmic scale and as a function of the energy. (b) Varshni plot for the near band edge emission and corresponding ZnO fitting parameters except for the Debye temperature which as explained in the text was taken from the literature. (c) UV peak emission intensity as a function of the inverse of temperature. The solid line represents the best fit to the data by the use of two activation energies E_1 and E_2. The dashed and dotted lines indicate the fits with a single activation energy E_1 or E_2, respectively.

$$E = E(0) - \frac{\alpha T^2}{(T - T_{\mathrm{Debye}})}$$

where $E(0)$ is the band gap at the absolute temperature $T = 0$ K, α the Varshni thermal coefficient and T_{Debye} the Debye temperature. The parameters obtained from the Varshni plot further confirms the high crystallinity of the NW with an alpha coefficient of 0.94 $\pm$ 0.02 meV K^{-1} comparable with ZnO thin films.[37] In order to reduce the number of fitting parameters and considering that we are dealing with nanowire,[38] we take for the Debye temperature, the bulk value.[39] The obtained bandgap energy at 0 K, $E(0) = 3.3642 \pm 0.0007$ eV together with the asymmetry of the peak strongly suggests surface defect bound excitons as observed by Wischmeier *et al.*[40–42] This is further confirmed by the Arrhenius plot where two activation energies are necessary to account for the $1/T$ dependance. The values we obtained are in agreement with those already reported in ZnO NWs.[36,40] Interestingly, we do not observe the neutral donor bound exciton peak (D^0X). This can be explained by a higher surface bound excitonic emission in our case as the size of the nanowires is on average about 2 to 4 times smaller than the NWs studied by Wischmeier *et al.*[41] which lower the volume related emission. From the integrated photoluminescence intensity measured at room temperature and 5 K, we estimate the internal quantum efficiency (IQE) of the UV emission. We found an IQE of 23% percent. High IQE observed in our ultra-thin ZnO NWs can be explained in terms of excitonic confinement. This value is higher than already reported values for unannealed samples. It is comparable to the IQE observed for samples annealed in hydrogen atmosphere[36] which is commonly used to enhance the luminescence properties of solution grown samples. Photoluminescence investigation confirms both the high cristallinity and high aspect ratio of the NWs.

C NW size control

In order to estimate the NWs diameter that one can achieve, a concentration dependent study was also performed. The concentration was varied between 0.018 M to 0.029 M. SEM images of typical urchin-like structures obtained for three different concentrations are shown in Fig. 6. For each concentration a histogram is plotted. The white line on the histograms represents a Gaussian fit. Higher concentrations lead to larger diameter NWs. The average size of the NWs obtained for the largest concentration, 0.029 M is 33 nm (Fig. 6a). With a

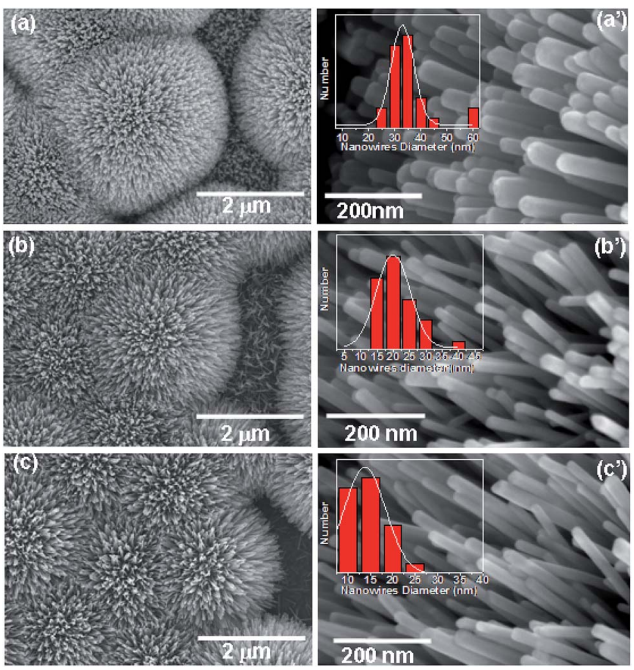

Fig. 6 SEM images of ZnO NWs grown as a function of varying solution concentration. Concentration of the solution used was (a, a') 0.029 M, (b, b') 0.02 M and (c, c') 0.018 M respectively. (a, b, c) are low magnification SEM images while (a', b', c') are magnified SEM images of the NWs showing the diameter dispersion of the NW size. The insets on the upper left hand corner in (a', b', c') show the diameter distribution of the NWs while the white line on the histograms represents the corresponding fitted Gaussian distributions.

decrease in the concentration of the solution, the average size of the NWs also decreases to 20 nm (Fig. 6b) and 14 nm (Fig. 6c) for the 0.02 M and 0.018 M concentrations respectively. Overall, the size dispersion of the NWs as evidenced by the full width at half maximum is quite narrow in all the three cases (10 nm typically). It is worth noting that urchin-like ZnO NW material has been grown on wafer scale as shown in the ESI (Fig. S1 and S2†).

Conclusions

Well-aligned, highly crystalline, small diameter ZnO NWs have been chemically synthesized on PS beads which were used as templates. The smallest NWs obtained had a diameter of about 9–10 nm with a length of around 200 nm. This dameter value leads to a density of NWs on a single PS bead as high as 8×10^4. Urchins were obtained using PS beads pre-coated with a ZnO seed layer. It was shown that the average diameter of NWs can be finely controlled in the size range of 10–30 nm by varying the concentration of the solution, smaller size being obtained with lower concentration. XRD patterns showed that the NWs had a wurtzite hexagonal structure and were highly crystalline. TEM images further proved that each NW was mono-crystalline. Temperature dependent PL spectra shows a dominant band edge emission (3.36 eV) and a weak deep level emission band centred around 2.31 eV. The strong NBE PL emission intensity compared to the deep level emission intensity implied a high crystal quality. This was further confirmed by an NBE emission internal quantum efficiency higher than 20%. In summary, we were able to perform templated growth of ultra-thin, highly crystalline, non-annealed NWs on PS beads using a bottom-up approach. These small-diameter 1D NWs integrated on 3D PS beads should further improve the performance of nanowire-based devices. One straight forward application of the highly luminescent urchin-like reported structures lies in chemo-sensing.[43] Furthermore such structures could facilitate the exploration of novel properties owing to both surface and confinement effects.

Acknowledgements

This work, through the MATISSE project, has been partially supported by the Champagne-Ardenne Regional council and the European Social Fund. The authors thank Mr Sergei Kostcheev for his help in SEM imaging using the NANOMAT platform equipment. It is also with great pleasure that we thank Mr Henry Pilliere and Mr Eric Berthier, (INEL Enterprise, Artenay, France) for the XRD measurements and Mr Alain Lusson (CNRS – GEMaC), Christophe Couteau (UTT – ICD/LNIO) and Michel Kazan (AUB) for fruitful discussions.

Notes and references

1 Z. Wang, *J. Phys.: Condens. Matter*, 2004, **16**, R829–R858.
2 W. Park and G.-C. Yi, *Adv. Mater.*, 2004, **16**, 87–90.
3 R. Konenkamp, R. Word and C. Schlegel, *Appl. Phys. Lett.*, 2004, **85**, 6004–6006.
4 J. Goldberger, D. Sirbuly, M. Law and P. Yang, *J. Phys. Chem. B*, 2005, **109**, 9–14.
5 H. Ng, J. Han, T. Yamada, P. Nguyen, Y. Chen and M. Meyyappan, *Nano Lett.*, 2004, **4**, 1247–1252.
6 W. Park, J. Kim, G. Yi and H. Lee, *Adv. Mater.*, 2005, **17**, 1393–1397.
7 H. Huang, S. Mao, H. Feick, H. Yan, Y. Wu, H. Kind, E. Weber, R. Russo and P. Yang, *Science*, 2001, **292**, 1897–1899.
8 J. Choy, E. Jang, J. Won, J. Chung, D. Jang and Y. Kim, *Adv. Mater.*, 2003, **15**, 1911–1914.
9 Z. Fan and J. Lu, *Appl. Phys. Lett.*, 2005, **86**, 123510/1–123510/3.
10 Q. Wan, Q. Li, Y. Chen, T. Wang, X. He, J. Li and C. Lin, *Appl. Phys. Lett.*, 2004, **84**, 3654–3656.
11 M. Law, L. Greene, J. Johnson, R. Saykally and P. Yang, *Nat. Mater.*, 2005, **4**, 455–459.
12 J. Baxter and E. Aydil, *Appl. Phys. Lett.*, 2005, **86**, 053114/1–053114/3.
13 C. Levy-Clement, R. Tena-Zaera, M. Ryan, A. Katty and G. Hodes, *Adv. Mater.*, 2005, **17**, 1512–1515.
14 J. Lee, K. Park, M. Kang, I. Park, S. Kim, W. Chom and S. Kim, *J. Cryst. Growth*, 2003, **254**, 423–431.
15 C. Geng, Y. Jiang, Y. Yao, X. Meng, J. Zapien, C. Lee, Y. Lifshitz and S. Lee, *Adv. Funct. Mater.*, 2004, **14**, 589–594.
16 S. Lyu, Y. Cheol, J. Lee, H. Ruh and H. Lee, *Chem. Mater.*, 2003, **15**, 3294–3299.
17 J. Wu and S. Liu, *Adv. Mater.*, 2002, **14**, 215–218.
18 M. Jeong, B. Oh, W. Lee and J. Myoung, *Appl. Phys. Lett.*, 2005, **86**, 103105/1–103105/3.
19 W. Park, D. Kim, S. Jung and G. Yi, *Appl. Phys. Lett.*, 2002, **80**, 4232–4234.
20 Y. Sun, G. Fuge and M. Ashfold, *Chem. Phys. Lett.*, 2004, **396**, 21–26.
21 X. Gao, X. Li and W. Yu, *J. Phys. Chem. B*, 2005, **109**, 1155–1161.
22 B. Cheng and E. Samulski, *Chem. Commun.*, 2004, 986–987.
23 B. Liu and H. Zeng, *Langmuir*, 2004, **20**, 4196–4204.
24 Y.-J. Kim, C.-H. Lee, Y. J. Hong and G.-C. Yi, *Appl. Phys. Lett.*, 2006, **89**, 163128-1–163128-2.
25 X. Lou, L. Archer and Z. Yang, *Adv. Mater.*, 2008, **20**, 3987–4019.
26 C. Levy-Clement and A. Hagfeldt, in *Nanostructured Materials for Solar Energy Conversion*, ed. T. Soga, Elsevier, 2006, pp. 444–484.
27 I. Gonzalez-Valls and M. Lira-Cantu, *Energy Environ. Sci.*, 2009, **2**, 19–34.
28 J. Elias, C. Clément, M. Bechelany, J. Michler, G. Wang, Z. Wang and L. Philippe, *Adv. Mater.*, 2010, **22**, 1607–1612.
29 J. Elias, C. Lévy-Clément, M. Bechelany, J. Michler and L. Philippe, *ECS Trans.*, 2011, **33**, 67–73.
30 J. Elias, L. Philippe, J. Michler and C. Lévy-Clément, *Electrochimica Acta*, 2011, **56**, 9532–9536.
31 A. Mosquera, D. Horwat, A. Rashkovskiy, A. Kovalev, P. Miska, D. Wainstein, J. M. Albella and J. L. Endrino, *Sci. Rep.*, 2013, **3**, 1714.
32 H. Yin, Q. Wang, S. Geburt, S. Milz, B. Ruttens, G. Degutis, J. D'Haen, L. Shan, S. Punniyakoti, M. D'Olieslaeger,

P. Wagner, C. Ronning and H. Boyen, *Nanoscale*, 2013, **5**, 7046–7053.
33 K. Vanheusden, W. Warren, C. Seager, D. Tallant, J. Voigt and B. Gnade, *J. Appl. Phys.*, 1996, **79**, 7983–7990.
34 X. Zhang, Y. Liu, J. Zhang, Y. Lu, D. Shen, X. Fan and X. Kong, *J. Cryst. Growth*, 2003, **254**, 80–85.
35 X. Huang, C. Tay, Z. Zhan, C. Zhang, L. Zheng, T. Venkatesan and S. Chua, *CrystEngComm*, 2011, **13**, 7032–7036.
36 X. Huang, Z. Zhan, K. Pramoda, C. Zhang, L. Zheng and S. Chua, *CrystEngComm*, 2012, **14**, 5163–5165.
37 Y. J. Zhanga, C. S. Xua, Y. C. Liua, Y. X. Liua, G. R. Wanga and X. W. Fan, *J. Lumin.*, 2006, **119–120**, 242–247.
38 R. Kumar and M. Kumar, *Indian J. Pure Appl. Phys.*, 2012, **50**, 329–334.
39 C. Boemare, T. Monteiro, M. J. Soares, J. Guilherme and E. Alves, *Phys. B*, 2001, **308–310**, 985–988.
40 L. Wischmeier, T. Voss, I. Rückmann and J. Gutowski, *Nanotechnology*, 2008, **19**, 135705–135710.
41 L. Wischmeier, T. Voss, I. Ruckmann, J. Gutowski, A. Mofor, A. Bakin and A. Waag, *Phys. Rev. B: Condens. Matter Mater. Phys.*, 2006, **74**, 195333-1–195333-9.
42 D. Stichtenoth, C. Ronning, T. Niermann, L. Wischmeier, T. Voss, C.-J. Chien, P.-C. Chang and J. G. Lu, *Nanotechnology*, 2007, **18**, 435701–435706.
43 R. Aad, V. Simic, L. Le Cunff, L. Rocha, V. Sallet, C. Sartel, A. Lusson, C. Couteau and G. Lerondel, *Nanoscale*, 2013, **5**, 9176–9180.